Mon. Not. R. Astron. Soc. **000**, 000–000 (0000) Printed 2 March 2000 (MN LATEX style file v1.4)

Coordinated Monitoring of the Eccentric O-star Binary Iota Orionis. Optical Spectroscopy and Photometry

Sergey V. Marchenko[1], Gregor Rauw[2⋆], Eleonora A. Antokhina[3], Igor I. Antokhin[3] Dominique Ballereau[4], Jacques Chauville[4], Michael F. Corcoran[5], Rafael Costero[6], Juan Echevarria[6], Thomas Eversberg[1], Ken G. Gayley[7], Gloria Koenigsberger[6], Anatoly S. Miroshnichenko[8], Anthony F. J. Moffat[1], Nidia I. Morrell[9], Nancy D. Morrison[8], Christopher L. Mulliss[8], Julian M. Pittard[10], Ian R. Stevens[10], Jean-Marie Vreux[2], Jean Zorec[11]

[1] *Département de Physique, Université de Montréal, C.P. 6128, Succursale Centre-Ville, Montréal, QC H3C 3J7, Canada, and Observatoire du Mont Mégantic*
[2] *Institut d'Astrophysique et de Géophysique, Université de Liège, 5, Avenue de Cointe, B-4000 Liège, Belgium*
[3] *Moscow State University, Sternberg State Astronomical Institute, Universitetskij Prospect 13, 119899, Moscow, Russia*
[4] *Observatoire de Paris-Meudon, DASGAL/UMR 8633, F-92125 Meudon Principal Cedex, France*
[5] *Universities Space Research Association/Laboratory for High Energy Astrophysics, GSFC, Greenbelt, MD 20771, USA*
[6] *Instituto de Astronomía, Universidad Nacional Autónoma de México, J. J. Tablada 1006, Colonia Lomas de Santa Maria, 58090 Morelia, Michoacán, México*
[7] *University of Iowa, Iowa City, IA 52245*
[8] *Ritter Observatory, The University of Toledo, Toledo, OH 43606, USA*
[9] *Observatorio de La Plata, 1900 La Plata, Argentina*
[10] *School of Physics and Astronomy, University of Birmingham, Edgbaston, Birmingham, B15 2TT, UK*
[11] *Institut d'Astrophysique, 98bis boulevard Arago, 75014 Paris, France*

Accepted ....; Received ....; in original form ....

ABSTRACT

With the objective of investigating the wind-wind collision phenomenon and supporting contemporaneous X-ray observations (cf. Pittard et al. 1999), we organized a large-scale, coordinated optical monitoring campaign of the massive, highly eccentric O9III+B1III binary Iota Orionis. Successfully separating the spectra of the components, we refine the orbital elements and confirm the rapid apsidal motion in the system. We also see strong interaction between the components during periastron passage and detect phase-locked variability in the spectrum of the secondary star. However, we find no unambiguous signs of the bow shock crashing on the surface of the secondary, despite the predictions of hydrodynamic simulations. Combining all available photometric data, we find rapid, phase-locked variations and model them numerically, thus restricting the orbital inclination to $50° \lesssim i \lesssim 70°$.

Key words:

1 INTRODUCTION

A significant fraction of massive stars can be found in binary systems, with high probability that both stars are nearly equally massive. Many of these early-type binaries have orbits with high eccentricity, especially those systems with longer periods. Systematic study of early-type, highly eccentric binaries provides insight to a variety of phenomena, including various aspects of the physics of colliding winds, tidal interactions and tidally-induced pulsations.

Study of colliding wind phenomena has greatly advanced in recent years. Following the pioneering study of Shore & Brown (1988), there have been major advances in several directions, both observational and theoretical. In the X-ray range, among the best studied massive colliding-wind WR+O systems are HD 193793 (Williams et al. 1990, Pollock et al. 1995) and γ^2 Velorum (Willis, Schild & Stevens 1995, Stevens et al. 1996). In the case of the strongly in-

⋆ Chargé de Recherches FNRS, Belgium

teracting O+O binaries, Corcoran (1996) presented a collection of X-ray observations, including the system of this study, ι Ori. Another system worth mentioning is Eta Carinae, now also believed to be a colliding wind binary with high eccentricity (Corcoran et al. 1998, Pittard et al. 1998).

Practically all recent optical/UV studies of colliding wind WR+O binaries are mentioned by Stevens & Howarth (1999). Examples of O+O-star systems include 15 Mon (Gies et al. 1997b); 29 UW Canis Majoris (Wiggs & Gies 1993; Bagnuolo et al. 1994); Plaskett's star (Wiggs & Gies 1992); and V729 Cyg (Rauw, Vreux & Bohannan 1999).

A wide variety of phenomena is predicted to occur in a massive binary system. They generally stem from a presumably strong interaction between the components, including enhanced mass loss, mass transfer between the components, various wind-wind collision effects, and stellar oscillations. Some of these phenomena lead to eruptive events, and others gradually modify the orbital parameters. For longer periods, the system is more likely to have a large orbital eccentricity, accentuating many of the effects, and making new ones appear. The interaction effects can be identified through the use of high resolution spectroscopy by searching for peculiar absorption or emission line profiles and their phase-locked variability. However, it is very likely that several interaction effects operate simultaneously in a given system, thus making it rather difficult to isolate the physical agent responsible for any particular component of variability. The problem is further complicated in relatively close binaries with high mass loss rates. Hence, it is also desirable to undertake a study of binaries where the mass loss rates are not so extreme, and where there is a good chance of isolation of the effects arising from the tidal interactions from the effects of the interacting winds.

To this end we have undertaken a multiwavelength campaign on the O-star binary Iota Orionis (HR 1889; HD 37043: O9III+ B1III), which is a highly eccentric (e = 0.764), relatively long period (P = 29.13376 d) binary. General properties of the system were reviewed by Stevens (1988) and by Stickland et al. (1987, hereafter SPLH87), who studied the system in order to determine whether the mass loss from either of the components is enhanced at periastron with respect to other orbital phases, finding no clear evidence for this effect. Gies et al. (1996) studied the system to determine whether non-radial oscillations driven by tidal forces at periastron are present, failing to detect the expected line-profile variability. Moreno and Koenigsberger (1999) developed a two-dimensional tidal interaction model including stellar rotation. The model was applied to ι Ori by following the vertical displacements and velocity amplitudes of each equatorial stellar surface element throughout the orbital cycle. It appears that with a radius for the primary star of 15 $R_\odot$, the tidal oscillation amplitudes might not exceed the limit of detectability, which could explain the non-detection of oscillation by Gies et al. (1996). The model enables one to predict the behavior of the stellar surface of both stars in the system. The growth and recession of the tidal bulges translate into photospheric line-profile and intensity variations, with the strongest variability in *iota Ori* expected to occur within a timespan of ±0.75 d around periastron passage (i.e., ±0.02 in phase).

Iota Ori has been recently observed by the *ASCA* satellite (c.f. Pittard et al. 1999) in order to investigate wind-wind collision phenomena. Here we present the results of the complementary optical campaign, organized in support of the X-ray observations.

2 OBSERVATIONS

2.1 Spectroscopy

New, high-quality spectroscopic observations of ι Ori were obtained at several locations:

1. Three high signal-to-noise (S/N$\sim$ 250 − 350 in the blue, S/N$\sim$ 350 − 450 in the red) spectra were obtained on September 1996,1997 using the 2.15 m telescope of Complejo Astronómico El Leoncito (CASLEO), San Juan, Argentina. The Cassegrain REOSC spectrograph, with a 400 l/mm grating and 1024×1024 CCD (24 × 24 μm pixel size) provided spectral coverage of $\lambda\lambda$ 3670-6120 Å and $\lambda\lambda$ 5830-8130 Å, and spectral resolution of ∼0.5-0.8 Å (blue-red regions, based on the FWHM of the interstellar lines). The initial processing was performed using the data reduction package written by J. Chauville.

2. Six spectra of ι Ori were collected around periastron passage on February 1997 using the Aurélie spectrograph fed by the 1.52 m telescope at Observatoire de Haute Provence (OHP), France. The spectrograph was equipped with a 1200 line/mm grating blazed at 5000 Å, providing a reciprocal dispersion of 7.6 Å/mm over a wavelength range from 6510 to 6710 Å. The detector was a Thomson TH7832 linear array with pixel size of 13 μm. The spectral resolution as derived from the FWHM of the calibration lines was ∼0.3 Å. A few additional observations were gathered with the same equipment on November 1998, but using a 1800 line/mm grating providing reciprocal dispersion of 5 Å/mm. All the OHP data were reduced in a standard way using the MIDAS software developed at ESO. To achieve a first order correction of the telluric absorption lines between 6500 and 6600 Å, a template of the telluric spectrum was built from observations of HD 36512 (ν Ori, B0 V) at very different airmasses. The mean S/N ratio in the continuum after correction for the telluric absorptions reaches ∼200 in the spectral range 6510 - 6600 Å and ∼500 elsewhere.

3. Multiple observations were obtained in Sept-Oct 1997 with a fiber-fed échelle spectrograph attached to the 1 m telescope of Ritter Observatory (USA) and equipped with a liquid-nitrogen-cooled Wright Instruments Ltd. CCD camera, which incorporates an 800 × 1200 EEV CCD05-20-0-202 thick sensor with pixel dimensions of 22.5 × 22.5 μm. The data reduction used Interactive Data Language (IDL) programs described in Gordon and Mulliss (1997). The spectral resolution element corresponds to an instrumental function of width about 4.2 pixels FWHM, i.e. 0.21 − 0.25Å. About 70Å of each of nine échelle orders was covered; in addition to Hα, features of interest in the spectra included OIII λ5592, CIII λ5696 and HeI λ5876. Under highly variable weather conditions, S/N ratios in the range 100–200 were achieved in exposure times ranging from 5 to 15 min. They were raised to $S/N \sim 200 - 350$ after triple-pixel rebinning of the original spectra. Experience with repeated high S/N ratio observations of K-giant radial velocity standards indicates that the velocity stability of this instrumentation is better than 1 km s^{-1}. Removal of the telluric absorption lines was performed using the spectrum of ζ Aql as a template.

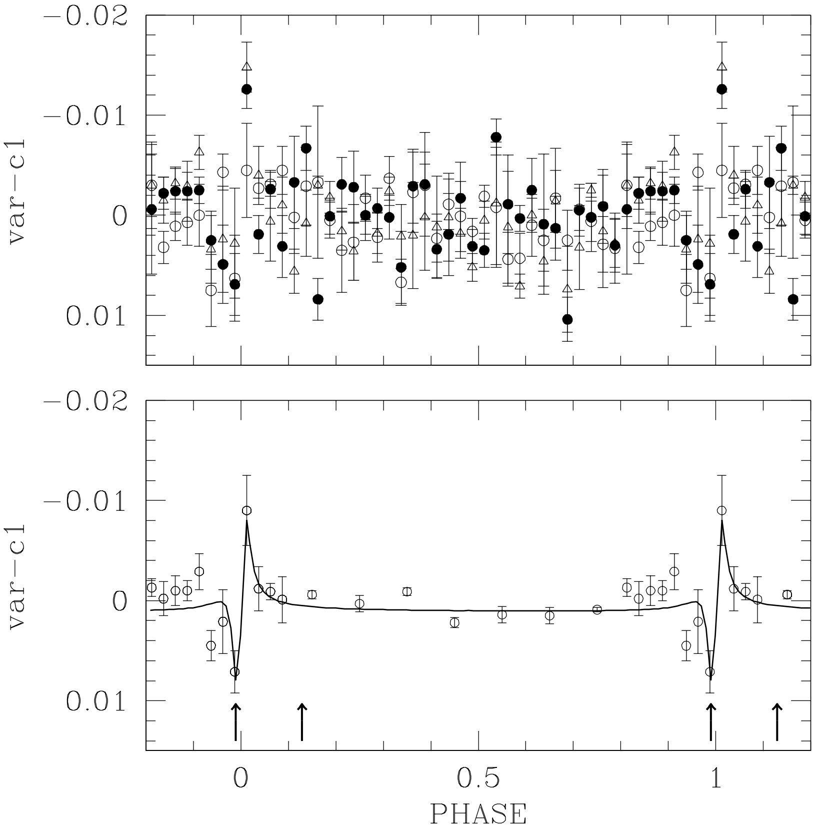

Figure 1. Upper panel: the individual differential U (triangles), B (open circles) and V (filled circles) observations of ι Ori, each with the mean subtracted off, and grouped in 0.025 phase bins (see text). Lower panel: the UBV-averaged light curve (open circles with 2σ error bars) of ι Ori folded with P_{orb} = 29.13376d and binned to 0.1 and 0.025 phase bins with the modeled light curve (solid line) corresponding to $i = 60°$ orbital inclination. The arrows point to the moments of potential eclipses.

4. Spectroscopic observations were carried out at the Observatorio Astronómico Nacional San Pedro Mártir (SPM), Mexico, on Sept 22 and 23, 1997 using an échelle spectrograph mounted on the 2.11 m telescope. The 2048 x 2048 Tektronics CCD detector provided $0.4 - 0.9$Å spectral resolution and $\lambda\lambda\,3200 - 7350$ spectral coverage. A total of 27 spectra were obtained, 8 on 22 Sept. and 19 on 23 Sept. with exposure times ranging between 40 and 180 secs. The spectra on each night were obtained within a timespan of less than 2 hours. An average spectrum was constructed for each night. The signal-to-noise ratio for the average spectrum ranges from 1000 in the blue to 600-800 in the red. The spectra were processed with IRAF†.

5. One spectrum (S/N∼300) was obtained at Observatoire du Mont Mégantic (OMM), Québec, Canada, using the 1.6 m telescope with the attached Cassegrain spectrograph and Loral 2048×2048 CCD. The 600 line/mm grating provided $\lambda\lambda 5770 - 7120$Å spectral coverage and $\Delta\lambda = 2.0$Å (3 pixels) resolution.

† IRAF is distributed by the National Optical Astronomy Observatories, operated by the Association of Universities for Research in Astronomy, Inc., under cooperative agreement with the National Science Foundation.

2.2 Photometry

Iota Ori was monitored in Johnson UBV optical filters at one of the automatic 25 cm telescopes in Arizona (cf. Young et al. 1991 for a general description). Between December 1996 and April 1998 we obtained 724 UBV observations of Iota Ori (about 240 data-points in each filter; 1-3 UBV cycles per night) with a typical accuracy for a single observation of 0.005-0.007 mag. Iota Ori was observed along with HR 1848 and HR 1840 as comparison and check stars, respectively, using a sequence of 10 sec integrations: check (ch, UBV) - sky (s, UBV) - comparison (c, UBV) - Iota (I, UBV) -c-I-c-I-c-s-ch.

In the absence of apparent (with amplitude $A \geq 0.01$ mag) long-term variations, we folded the individual U,B,V data with P_{orb} = 29.13376d and E_0 = HJD 2451121.658 (Stickland et al. 1987 and below), binned them to 0.1 phase bins and combined the binned U,B and V light curves by simple averaging after removal of the mean in each filter, as the differences between the binned U,B and V light curves did not exceed the observational errors. We immediately noticed flux variations taking place around periastron passage (phase 0.0). To provide better time resolution and improve the accuracy even further, we again phased the individual U,B and V data and binned them to 0.025 phase bins, then ordered and trimmed the data within each bin for each filter, taking out the upper and lower 10% (B and V) or 15% (U) of the data (as judged by a median value of the given

Table 1. Measured radial velocities

HJD-2450000	Observatory[a]	Phase	Primary RV ($km\,s^{-1}$)	Primary σ_{RV} ($km\,s^{-1}$)	Primary RV_{calc} ($km\,s^{-1}$)	Secondary RV ($km\,s^{-1}$)	Secondary σ_{RV} ($km\,s^{-1}$)	Secondary RV_{calc} ($km\,s^{-1}$)
347.883	CASLEO	0.441	40.6	0.2	41.4	28.8	15.4	2.7
505.314	OHP	0.844	84.8	2.0	84.2	-90.8	11.9	-72.1
506.375	OHP	0.881	84.6	2.5	87.3	-115.0	17.7	-77.5
507.369	OHP	0.915	84.4	2.5	88.1	-97.4	25.8	-78.9
508.353	OHP	0.949	79.4	2.5	80.4	-86.2	16.6	-65.5
509.318	OHP	0.982	24.3	1.8	19.9	33.6	11.9	40.3
510.379	OHP	0.018	-125.9	6.4	-132.8	290.8	11.6	307.4
704.876	Ritter	0.695	65.3	2.8	68.7	-23.0	22.4	-45.0
704.893	CASLEO	0.695	73.1	0.7	68.7	-46.6	18.4	-45.0
706.899	CASLEO	0.764	75.0	2.0	79.9	-70.7	15.7	-64.6
709.928	Ritter	0.868	92.6	2.8	86.3	-82.3	20.7	-75.8
712.895	Ritter	0.969	54.1	1.9	57.3	-2.1	27.1	-25.1
712.903	Ritter	0.970	50.8	4.7	56.8	10.6	42.2	-24.2
713.901	Ritter	0.004	-115.1	3.6	-116.8	291.1	12.9	279.4
713.924	SPM	0.005	-122.7	1.9	-120.1	279.5	2.2	285.2
714.932	SPM	0.039	-101.9	1.8	-99.3	255.7	2.1	248.8
715.928	Ritter	0.074	-45.2	5.3	-58.6	171.4	6.2	177.6
717.915	Ritter	0.142	-15.6	3.8	-18.4	92.9	21.6	107.3
719.810	OMM	0.207	-6.0	8.0	2.3	81.2	16.0	71.1
724.914	Ritter	0.382	37.0	2.6	33.9	27.8	16.3	15.8
725.901	Ritter	0.416	43.9	5.7	34.3	25.0	13.4	15.1
732.877	Ritter	0.655	74.3	1.0	64.7	-44.8	22.1	-38.0
1136.580	OHP	0.512	39.8	1.1	49.6	3.4	10.9	-11.6
1137.574	OHP	0.546	49.4	1.1	53.3	-2.7	10.9	-18.1

[a] CASLEO - Complejo Astronómico El Leonsito (Argentina); OHP - Observatoire de Haute-Provence (France); SPM - the San Pedro Mártir Observatory (Mexico); OMM - Observatoire du Mont Mégantic (Québec); Ritter - the Ritter Observatory (USA).

bin) and calculating the average values for the binned and trimmed data in each filter. Then we averaged the individual U,B and V light curves, thus reaching an accuracy of $\sigma \lesssim 0.001 - 0.002$ mag for a binned data point. Detecting no significant variability at phases 0.1-0.8, we increased the bin size to 0.1 while combining the individual U,B,V light curves at phases 0.1-0.8, however keeping the sufficiently high 0.025 phase resolution around periastron (Fig. 1). The 0.025 phase resolution was chosen after some experimentation as a reasonable compromise between the simultaneously required high accuracy ($\lesssim$0.002 per bin) and high time resolution. Inspecting the average light curve in Fig. 1 one may notice the somewhat larger error bars for the points closest to phase zero. One may also note the deviation of the B light curve from the U and V data around $\phi = 0.9625$ and $\phi = 0.0125$ (Fig. 1, upper panel). It is tempting to assume that enhancement of the intrinsic variability of the system around periastron could be a possible source of the deviations. This is supported by the fact that the individual light curves comprising the data were taken at different orbital cycles. Indeed, the time sampling of the 0.025 phase bins at $\phi = 0.9625$ and $\phi = 0.0125$ is slightly different: the $\phi = 0.9625$ bin contains 5 observations in U and 5 in V of the same time sequence, but only four B points; the $\phi = 0.0125$ bin includes five U, four V (all times are overlapping with U) and six B points. With the current data in hand, the suggestion of the enhanced intrinsic variability during periastron passage may be regarded only as tentative, pending acquisition of the data of much higher quality.

3 RADIAL VELOCITY MEASUREMENTS

In order to measure as precise RV's as possible, we first constructed a template for the primary star. Gaussian (OIII 5592, CIV 5801,5812) or Voigt (HeI lines, Hα) profiles were fitted to the primary's lines at phases when the primary and secondary spectra are well separated (i.e. around periastron passage). We created a zero-approximation artificial spectrum of the primary by assigning to its components the averaged half-widths and intensities of the observed lines and placing all the artificial components at the laboratory wavelengths. This artificial spectrum was properly Doppler-shifted and compared to the composite (primary+secondary, originally observed) spectra at different phases, with emphasis on the parts of the composite profile the least affected by the presence of the secondary. We quickly realised that this artificial spectrum of the primary generally underestimates the primary's line depths, if based solely on the data taken around periastron. Measuring line depths at out-of-periastron phases where the lines of the secondary, nevertheless, are sufficiently displaced from the primary's profiles and accordingly adjusting the fitted parameters (mainly the line intensities), we finally constructed a compromise version of the artificial spectrum of the primary. We found the Hα profile of the primary to be blue-shifted relative to the OIII and HeI lines. This phenomenon (sometimes referred to as Balmer progression; cf. the discussion in Hutchings 1968) is probably indicative of an expanding atmosphere. Hence, we applied a $\Delta RV = -28.4\,\mathrm{km\,s^{-1}}$ correction to the laboratory wavelength of Hα while creating the final version of the artificial spectrum of the primary.

This artificial spectrum was then cross-correlated (the 'fxcor' task in IRAF) with the individual observed composite spectra. The so measured RVs of the primary component were subsequently adjusted (usually by $\Delta RV < 20\,\mathrm{km\,s^{-1}}$) to provide the best match for the parts of the composite profile where the secondary's presence was assumed to be negligible (line wings of the composite profiles for the phases 0.3-0.7; red side for the phases 0.7-0.9, etc.). Subtracting the appropriately shifted artificial spectrum of the primary from the composite spectra, we thus obtained a set of secondary spectra. These were then mutually cross-correlated, appropriately shifted and combined into a mean spectrum of the secondary. While constructing this secondary template, we omitted all the spectra taken around periastron, in the expectation that they could be affected by phase-locked spectral variability at those phases. Then we cross-correlated the secondary template with the individual difference spectra (composite spectrum minus appropriately Doppler-shifted artificial spectrum of the primary) to obtain more robust velocity estimations for the secondary component. Subtracting the primary(secondary) template from the appropriately (orbital motion) shifted composite spectra, we obtained a collection of phase-resolved secondary(primary) spectra to look for any phase-related profile variability. In Table 1 we list: the HJD dates calculated for the mid-exposure times; the source of the data; the orbital phases; the heliocentric RVs and corresponding $\sigma(RV)$ as measured via cross-correlation, along with the calculated RVs. We note that the restored secondary and primary profiles are in fair agreement with the profiles obtained by Gies et al. (1993; 1996). Some of the quoted RV errors may seem unrealistically small, as they are based exclusively on the results of the cross-correlation procedure, thus neglecting the additional source of errors stemming from the uncertainty in the 'absolute', zero-point wavelength calibration. Unfortunately, the latter error cannot be uniformely assessed from the available data, as for a given observatory they sometimes comprise only 1-3 spectra covering different wavelengths. As we already mentioned, the velocity stability was better than 1 km s^{-1} in the spectra obtained at Ritter Observatory. As for the rest of the spectra, the measurements of the interstellar lines (whenever possible) showed random deviations not exceeding 10 km s^{-1}. The overall uniformity of the data set can be evaluated by comparing the data plotted in Fig. 2, where different symbols correspond to different observatories. In the following RV analysis we refer to the cross-correlation errors only.

4 ORBITAL PARAMETERS

A revised orbital solution for ι Ori was derived from our RV measurements using an improved version of the algorithm of Wolfe et al. (1967) and using $1/\sigma$ RV weights (cf. Table 1).

Table 2. New orbital solution derived from our RV measurements. The quoted uncertainties are 1-σ errors.

	Primary	Secondary
P (days)	29.13376(fixed)	
γ (km s^{-1})	31.3 ± 1.2	20.4 ± 2.1
K (km s^{-1})	111.9 ± 2.5	195.7 ± 4.3
q $=M_1/M_2$	1.749	
e	0.764 ± 0.007	
$\omega(^\circ)$	130.0 ± 2.1	
T_0 (HJD-2450000)	1121.658 ± 0.046	
$M \sin^3 i\,(M_\odot)$	15.0	8.5
$a \sin i\,(R_\odot)$	41.5	72.7

The problem of relatively slow convergence of the algorithm for orbits with $e \gtrsim 0.8$ was circumvented by choosing an appropriate number of terms in the asymptotic expansion, 4 terms in our case. Since the radial velocities of the secondary are probably affected by line profile variations (see below), a simultaneous determination of all the orbital parameters from the data of both components seems inappropriate. We have thus obtained the orbital solution of the primary independently of the secondary's RVs. The secondary's RV curve was then derived after fixing the values of e, ω and T_0 as determined for the primary star alone, with amplitude and apparent systemic velocity as the only free parameters.

Since there is strong evidence for apsidal motion in ι Ori (SPLH87), it is problematic to combine datasets from very different epochs to derive an improved orbital period. Therefore, we have restricted ourselves to the combination of our data with the most recent RV dataset available in the literature (Hilditch et al. 1991), thus obtaining the most probable period of 29.13434 ± 0.00020 d. Since the longitude of periastron increases with time, this value should provide an upper limit to the actual orbital period. We note however, that at any orbital phase the primary's RVs from the Hilditch et al. (1991) dataset are systematically closer to the apparent systemic velocity than our data. Hilditch et al. adopted an empirical correction to account for the effects of spectral-line blending on the RVs of the primary. It could be that this correction is not large enough to account for the entire effect of the blending. In the following, we will therefore focus on the analysis of our new dataset alone.

We have tested several assumptions on the orbital period, adopting either the value 29.13376 d of Stickland et al. (SPLH87) or using the period of 29.13434 d, as derived above. Both options yield orbital elements that overlap within their errors. The solution obtained adopting the period proposed by SPLH87 is given in Table 2 and displayed in Figure 2.

The eccentricity of our solution is in excellent agreement with the value from SPLH87. A rather unexpected finding is the difference in the apparent systemic velocities of the two components ($\gamma_1 - \gamma_2 = 10.9\,\mathrm{km\ s^{-1}} \simeq 5\,\sigma$). Fitting the RVs of the secondary as quoted by SPLH87, we find that the same discrepancy also exists in their dataset. This phenomenon is quite common in evolved O + O binaries, and is usually attributed to the influence of a stellar wind on the formation of absorption lines. In this interpretation, the component with the strongest wind should display the

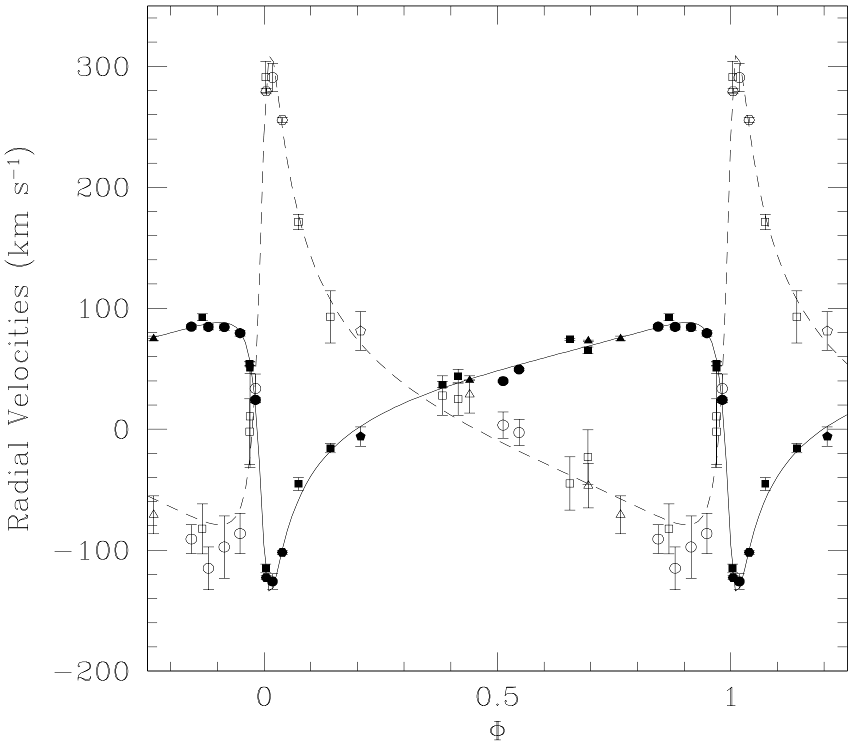

Figure 2. Radial velocity curve of ι Ori as determined from our RV measurements. The filled (open) symbols indicate the RVs of the primary (secondary) component: triangles - CASLEO; circles - OHP; pentagons - OMM; squares - Ritter; hexagones - SPM.

most blue-shifted absorptions. However, in the case of ι Ori, it is the secondary component with the presumably weaker wind which has the bluer apparent systemic velocity. We therefore believe that the γ-velocity difference in ι Ori could be an artifact resulting from the phase-locked line profile variability of the secondary star (see Section 5).

Considering apsidal motion, we notice that the longitude of periastron in our solution ($\omega = 130.0^{\circ} \pm 2.1^{\circ}$) is larger than the value (126.2°) obtained from an extrapolation of the empirical linear relation given by SPLH87. We have therefore performed a least square linear fit in time to all the available measurements of ω (Plaskett & Harper 1909, Pearce 1953, Miczaika 1951, SPLH87, Hilditch et al. 1991, this paper). The best fit corresponds to a rate of apsidal motion $\dot{\omega} = (0.00049 \pm 0.00003)^{\circ}$/day, slightly larger than the value derived by SPLH87 (0.00041°/day).

The mass ratio $q = m_1/m_2 = 1.75$ in our solution is lower than the value found by SPLH87, $q = 2.05$. However, since this difference arises from an increase of K_1 and a decrease of K_2 in our data compared to SPLH87, the total semi-major axis of the system $a \sin i = 114.2\,R_{\odot}$ is nearly unchanged with respect to the results of SPLH87 ($112.8\,R_{\odot}$) and therefore our revision of the orbital elements of ι Ori should have little impact on the modelled colliding wind effects (Pittard 1998). Concerning the predicted proximity effects (Stevens 1988; Moreno & Koenigsberger 1999), we notice that the downwards revised mass ratio will lead to a smaller critical volume of the primary near periastron than expected from the SPLH87 solution. Hence, the predicted deformations of the primary could be somewhat larger than the model estimates (Moreno & Koenigsberger 1999).

5 DISCUSSION: OBSERVED PROXIMITY EFFECTS

5.1 Spectroscopy

In ι Ori the phase-locked profile variations induced by the rapid change of separation between the components during periastron passage must be disentangled from the stochastic line variability affecting the primary spectrum. The latter type of variability was not detected in spectra acquired within the same night, but was clearly present as a night-to-night and cycle-to-cycle component. However, in ι Ori these stochastic variations are generally of small intensity and usually confined to the cores of the profiles (cf. Gies et al. 1993).

Calculating the standard deviations for all but two (phases 0.0-0.1 -see below) Hα profiles, we found that the stochastic component can cause line profile variations with full amplitude up to 3% (referring to the continuum). When possible, we minimized the influence of this stochastic variability via: (a) averaging the spectra taken at different cycles; (b) grouping the spectra within wide phase bins. Following this simple recipe, we immediately find that all the secondary's line profiles undergo dramatic changes during periastron passage (Fig. 4). To demonstrate this, all the individual profiles were Doppler-shifted to the frame of the secondary in accordance with the secondary's orbit and grouped within 3 phase bins: 0.0-0.1, 0.1-0.9, 0.9-1.0. We found the profiles to be somewhat depleted before periastron ($\phi = 0.9 - 1.0$) passage and greatly enhanced right after that ($\phi = 1.0 - 1.1$) compared to the 'neutral' mean profiles taken at $\phi = 0.1 - 0.9$. The additional emission at $v = -(500 - 300)$ km s^{-1} is an artifact created by the phase-

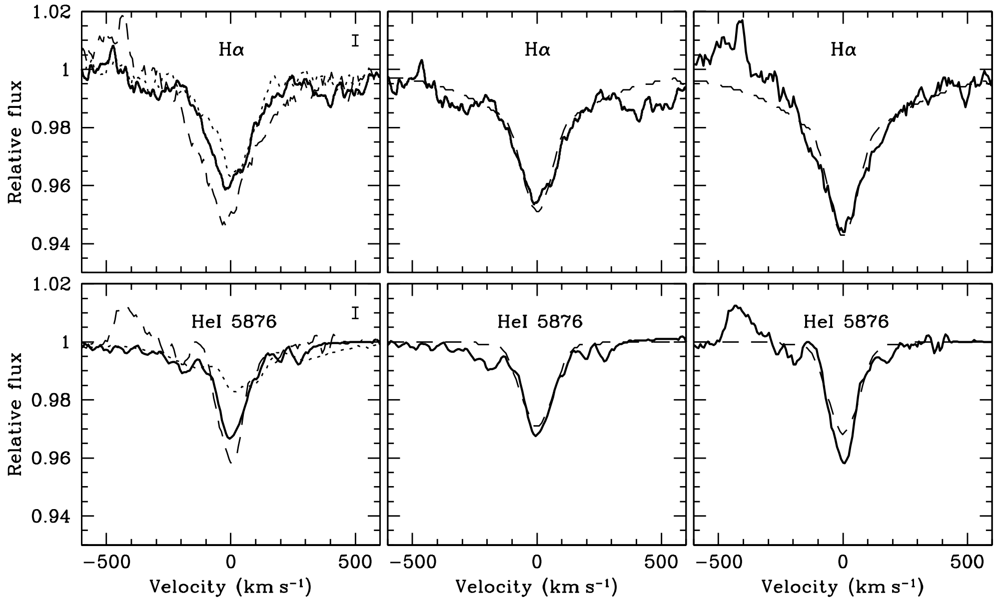

Figure 4. Phase-averaged line profiles of the secondary component. Left panel: full line - phases 0.1-0.9 (each profile: mean of 10 HeI profiles and 11 Hα profiles); dotted line - phases 0.9-1.0 (mean of 2 HeI profiles and 5 Hα profiles, respectively); long-dashed line - phases 0.0-0.1 (mean of 4 HeI profiles and 3 Hα profiles, respectively). Typical 2-σ error bars are shown in upper right corners of the panel. Middle panel: full line - phases 0.1-0.9, observed profiles; long-dashed line - modeled profiles. Right panel - the same as in middle panel, but for phases 0.0-0.1.

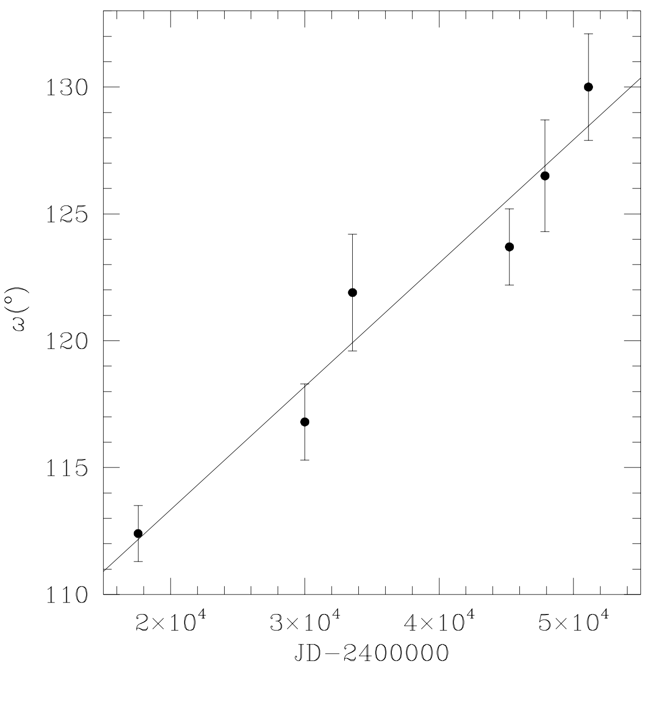

Figure 3. Least square fit to the observed variations of the longitude of periastron in ι Ori (see text).

related variability of the primary's profiles (see below). Note that at phases $\phi = 0.9 - 1.0$ (and *only* around these phases) we are able to look at the rear side of the secondary star, which is not affected by the flux coming from the primary.

The deepening of the secondary's profiles after periastron has been noted by Gies et al. (1996) and could be related to: (a) illumination of the secondary component's hemisphere by the nearby and far more luminous primary star and, additionally, to (b) the Struve-Sahade effect, which, among other possibilities, might be caused by heating of the secondary by the radiation coming from the wind-wind collision zone (either back-scattered photospheric flux or direct X-ray irradiation: Gies et al. 1997a). To verify this hypothesis, we calculated grids of the HeI 5876 and Hα line profiles using the non-LTE code TLUSTY (Hubeny & Lanz 1995) for an H (15 levels) and He (14 levels) atmosphere, turbulent velocity of 5-25 km s^{-1} (Hubeny & Lanz 1992), gravitational acceleration of $log\, g = 4.1$ (cgs; in correspondence with the values derived from the light curve fit; see below), rotational velocity $v_e \, sin\, i = 50 - 100$ km s^{-1}, primary/secondary flux ratio in the optical $I_1/I_2 = 7.9$ (see section 5.2) and variable effective temperatures, keeping fixed solar chemical composition. Apparently, the outcome of the modeling should depend on the initial choice of $log\, g$ and chemical composition. However, our intention will be to follow the differential, phase-related changes in the surface temperature. We are aware that the absolute values might be uncertain at a level exceeding the quoted errors. However, we argue that the differences in the temperatures are less sensitive to the choice of He/H ratio, v_{turb}, $log\, g$, etc., as those parameters, once chosen, remain fixed for all the spectra. Fine tuning of the model providing accurate absolute temperatures could be done only via incorporation of wide-range spectral data with an adequate coverage of orbital phases. Unfortunately, we lack such data.

The modeling provides very good fits (Fig. 4) for the averaged profiles corresponding to the 0.1-0.9 phases, with $T_{eff} = 25000 \pm 1000$ K, in coincidence with $T_{eff} = 24000 - 25400$ K for B1III-V stars [Schmidt-Kaler 1982; note that the small radius of the B1 component as derived from the light curve fitting (below) has a better correspondence with luminosity class V than the previously accepted III], $v_{turb} = 25$ km s^{-1} [‡] and $v_e\, sin\, i = 75 \pm 10$ km s^{-1} (in the range of the previously published $v_e\, sin\, i$ estimates for the secondary, $v_e\, sin\, i = 68-80$ km s^{-1} : Gies et al. 1993, 1996; Howarth et al. 1997). Despite the relatively low quality of the fits (Fig. 4) to the phase 0.0-0.1 profiles (fixed $v_{turb} = 25$ km s^{-1} and $v_e\, sin\, i = 75$ km s^{-1}), we are able to conclude that the $H\alpha$ profile can be fitted only assuming much lower $T_{eff} = 19000 \pm 1000$ K. At these phases, there is no possibility to match the observed HeI profile, with its central part being far too strong for any reasonable choice of T_{eff}. Note also the broadening of the observed $H\alpha$ profile.

It is clearly futile to attempt to find precise T_{eff} values for the asymmetric, peculiar shaped (especially HeI 5876 line) profiles corresponding to 0.9-1.0 phases. They are indicative of $T_{eff} \gtrsim$28000 K. Although the absolute values of the temperatures might be somewhat biased by the initial choice of parameters, there is little doubt that we observe fairly large, phase-dependent line profile variations, which we attempted to model as photospheric temperature variations. We may conclude that they cannot be caused by the changing separation between the components, as the more luminous primary has practically negligible influence on the secondary's profiles, being of comparable T_{eff}; we have been able to check this by introducing an external illumination factor in TLUSTY.

Could the variations be due to the crashing of the bow shock onto the secondary? Note that from general considerations one expects to see significant imbalance in the wind's momenta (up to 100 times: SPLH87). In a simplistic approach, at $\phi = 0.0 - 0.1$ the shock zone is seemingly detached from the secondary's atmosphere; otherwise, the secondary's profiles would be significantly depleted, as the crashing bow shock would completely engulf the Hα formation zone, reaching the region of formation of HeI lines as well, and raising the inside-zone temperature by ~two orders of magnitude. However, the real situation might be more complicated, with everything related to the relaxation timescale for the zone of the shocked gas. This may range from hours to days, critically depending on the poorly known velocity of the primary's wind in the vicinity of the secondary's surface: any extrapolation of the widely accepted β-velocity law (cf. Pittard et al. 1999) is very risky, owing to the fact that the wind braking effect (a sudden deceleration of the primary's wind by the radiation field of the secondary: Gayley et al. 1997; see also the discussion in Pittard et al. 1999) is presently only schematically accounted for. Assuming that the zone of shocked gas can settle to some equilibrium within hours (the assumption being supported by the extremely efficient radiative cooling in the relatively high-density region of the secondary's atmosphere), we proceed by suggesting that the observed 'low-temperature' Hα profile at $\phi = 0.0 - 0.1$, as well as the anomalously strong HeI 5876 line, can be formed *inside* the wind-wind collision zone - more specifically, in the decelerated and cooled part of the primary's wind. In a rather speculative vein, this assumption may be counteracted by two arguments: (i) The dynamical equilibrium reached by the shocked gas could be continuously violated during periastron passage, when the rapidly changing separation can significantly affect the ram pressure balance. (ii) The rapidly cooled wind-wind collision zone is prone to large-scale, turbulent gas motions (Stevens, Blondin & Pollock 1992; Walder & Folini 1998). It remains to be seen that the apparently smooth *absorption* profile can be formed in such a violent, fractalized medium; however, note the apparent broadening of the Hα profile at phases 0.0-0.1 comparing to the model fit (Fig. 4).

More conventional solutions of the non-crashing paradox suggest: either an extremely extended acceleration zone in the wind of the primary, or an unexpectedly strong wind braking effect. Another, though rather debatable, possibility to change the wind momentum ratio in favor of the secondary, thus lifting the shock from the secondary's surface, is to assume that the primary's wind velocity can be reduced by strong tidal interaction effects (a somewhat higher mass loss rate with the related significant change in acceleration rate in the outer region of the primary's wind). However, the change in wind velocity would lead to a significant change in the hardness of the X-ray emission near periastron. The fact that we do not see this (Pittard et al. 1999) either implies that the X-ray emission does not come from the wind interaction region, or that there is something wrong with our expectation of a *considerably* changed wind structure at phase 0.0.

The phase-locked profile variations in the primary's spectrum are more subtle and are evident only in the spectra taken around $\phi = 0.00 \pm 0.01$ (Fig. 5). We confirm the finding of Gies et al. (1996): for a short time the central parts of the primary's profiles are partially filled in by line emission probably arising in a tidal stream created by the gravitational pull of the secondary component. The variability in the red wing of the primary's HeI 5876 profile is caused by the phase-related changes in the secondary's spectrum (as above). Simulations of the tidal stream emissivity will require incorporation of radiation transfer in a perturbed, three-dimensional stellar atmosphere, which is far beyond the scope of this paper. It is quite surprising that practically all interaction effects are restricted to such a short time interval: note also the optical light curve maximum (see below) and the 'spike' in the X-ray light curve (Pittard et al. 1999). However, it is consistent with the results of the tidal

[‡] The chosen value of v_{turb} seems rather high. However, our choice was motivated not only by quality of the model fits, but also by the matter of convergence of the 'low- temperature' models, $T_{eff} = 15000-20000$ K. This particular choice does not affect much the final results, as we compare the rotationally broadened spectra of $v_e\, sin\, i \sim 3\, v_{turb}$; additionally, our instrumental profile has $v_{instr}(FWHM) \sim v_{turb}$. This rotational and instrumental broadening make the final results rather insensitive to the initial choice of v_{turb} anywhere within the 5-25 km s^{-1} interval.

interaction model of Moreno and Koenigsberger (1999), who find that the time-span over which mass motions on the tidal bulge have velocities larger than 1 km s^{-1} is $\sim$10 hours.

We found that a relatively strong ($\sim$ 5% of the continuum) CIII 5696 emission line follows the primary's orbit, with some indication of phase-related variability. However, the emission was placed too close to the edge of the echelle order to achieve sufficient accuracy for quantifying those changes. Note that this line appears in emission in practically all luminous late-type O stars (Conti 1974; Walborn 1980).

5.2 Photometry

To interpret the rapid light curve variability taking place during periastron passage (Fig. 1), we applied a numerical code (Antokhina & Cherepashchuk 1994; Antokhina 1996) designed to calculate a light curve for an eccentric orbit under the standard assumptions (Wilson 1979) that: (a) the shapes of the stars coincide with instantaneous equipotential Roche surfaces at all orbital phases, and (b) the stars retain constant volumes during orbital revolution. The model takes into account changes in shapes of the components, mutual radiative heating, and possible geometrical eclipses. Note that at such a large eccentricity ($e = 0.76$), the standard Roche model is far from being well justified. Near periastron, strong tidal interaction and resulting instabilities may distort the shapes of the components. In fact, we see some signs of such interaction: the profile variability in the primary component (Fig. 5) and rapid change of the longtitude of periastron. Stevens (1988) used the equipotential Roche surface assumption and derived the variation in the (maximum) radius of iota Ori's primary star between periastron and apastron, obtaining a difference of 0.39 $R_\odot$ in the radii at these two orbital phases. However, Moreno and Koenigsberger (1999) obtain a change in the radius of only 0.02 $R_\odot$ from the solution of the equations of motion of the surface elements in the equatorial region, assuming that the stellar radius is 15.8 $R_\odot$. Furthermore, the shapes of the stars at periastron differ from those at other phases, having prolate spheroidal appearance. Thus, the following results obtained with the standard Roche model should be treated only as indicative, pending the inclusion of the precise shapes of the stars into the light curve calculation method.

As model input we use the known spectroscopic values of $M_1\,sin^3 i$, $M_2\,sin^3 i$, P, ω, e, T_0 (Table 2), as well as averages of the previously published data on $v_e\,sin\,i$ = 110 km s^{-1} (primary) and 70 km s^{-1} (secondary), characteristic values of T_{eff} = 32500K (primary) and T_{eff} = 24000K (secondary). Gravity darkening coefficients $\beta_1 = \beta_2 = 0.25$ and albedos $A_1 = A_2 = 1$ are assumed as typical for early type stars. The square-root limb darkening law (Van Hamme 1993) is used for calculations of the limb darkening. We choose $\lambda_0 = 4400$Å for the calculated monochromatic light curve, in correspondence with the central wavelength of the photometric B band.

With the majority of the fundamental parameters fixed, we place restrictions on the orbital inclination. We start from calculating a grid of models with $\Delta i = 10°$ (afterwards changing to $\Delta i = 5.0°$ around the optimal i value), using μ_1, μ_2 (the Roche lobe filling factors for the primary and secondary, respectively, calculated for the moment of periastron passage) as free parameters and attempting to find the best fit to the observed light curve using Fisher's statistical criterion (Balog et al. 1981). As it turns out, the optimal solution is not very sensitive to the choice of i, which can be partially explained by the extremely small amplitude of the light curve and, as a consequence, by the *comparatively* large observational errors ($\sim 0.001 - 0.002$ mag/point!). However, the primary reason for this is that the light variations are caused exclusively by tidal deformations of the components, not by eclipses. In the absence of eclipses, changes in inclination may be, to a large degree, compensated by appropriate changes in radii, so that the observations do not further constrain the radii and the inclination. In almost all cases one has to choose between 2 or more statistically equal solutions: usually, one with small μ_1 and large μ_2 and the other(s) with opposite μ_1/μ_2 ratio. Our selection was based on the fact that the primary star is bigger, hotter, more massive and more luminous, with $\Delta\, m = 2.0 \pm\, 0.2$ mag in the optical (SPLH87). We list the derived values in Table 3, where μ_1, μ_2 are the Roche lobe filling factors at periastron; a is the semi-major axis; F_1 and F_2 are the ratios of surface rotation rate to synchronous rate for the primary and the secondary, respectively, calculated as $F_j = \omega_j/\omega_{kepl} = [v_j/R_j]/[2\pi/P]$, where v_j are taken from the known $v_j\ sin\ i$; L_1, L_2 are the bolometric luminosities of the components and $\Delta\ (o-c)$ is the normalized deviation for a given model of the light curve. At a confidence level of 1% (referring to Fisher's statistics), the critical value is $\Delta\ (o-c) = 1.90$, and $\Delta\ (o-c) = 1.59$ at 5%. This provides a 99% confidence interval for the inclination, $50° \lesssim i \lesssim 70°$ with the optimal value at $i = 60°$ (the

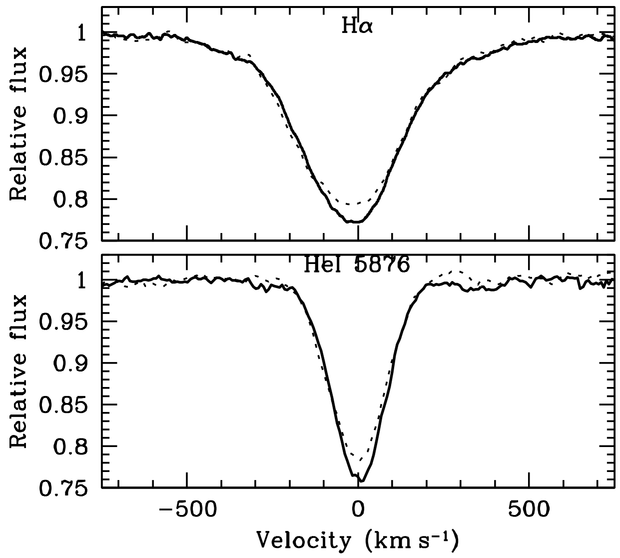

Figure 5. Phase-averaged line profiles of the primary component: full line - all phases except $\phi = 0.003 - 0.005$ (mean of 12 HeI profiles and 17 Hα profiles); dotted line - phases 0.003-0.005 (mean of 2 spectra).

modeled light curve is shown in Fig. 1) and corresponding $R_1 = 8.3 \pm 0.8\,R_\odot$, $R_2 = 5.4 \pm 1.4\,R_\odot$, and $M_1 = 23.1\,M_\odot$, $M_2 = 13.1\,M_\odot$, with the masses being in reasonable agreement with the spectral types of the components. The derived radii are substantially smaller than the estimates from SPLH87, where the radii were calculated under the questionable assumption that the minimum in the light curve that is observed before periastron passage corresponds to a grazing eclipse. In our model, for the optimal value of $i = 60^\circ$ the observed variations could be interpreted as induced by the component's proximity alone, without eclipsing. However, smaller radii imply much smaller tidal deformations (Moreno & Koenigsberger 1999) and it is not clear whether such small deformations would produce the observed variations.

The new values of the radii point to luminosity class V rather than the traditionally assigned III. This immediately poses an additional problem: the system, judging by its total luminosity (case $i = 60^\circ$, Table 3), is a factor of 3 fainter than can be deduced from the mean distance modulus of the Ori OB1 association, considering ι Ori as a member (c.f. SPLH87). However note that differences in the individual distance moduli of the association members may reach ± 1 mag (Humphreys 1978).

We reiterate our conclusion reached in the previous section that heating by the *luminous* primary component cannot cause the observed phase-locked profile variability of the secondary star. Within our model, the calculated rise in the secondary's surface temperature during periastron passage never exceeds 150 K.

The calculated asynchronous rotation rates deserve additional comment. As the values of F_i cannot be fixed initially, depending non-linearly on μ_i, they have to be calculated iteratively. For a given μ_i we set $F_i = 1.0$, then calculate the equipotential surface, its volume and mean radius, and, finally the new F_i. As these new F_i would deviate from 1, we re-solve the equation for the equipotential surface for the new F_i, repeating the process until convergence. This procedure ensures that values of $v_e\ sin\ i$ in our model match the observed values, $\sim 110\,\mathrm{km\ s^{-1}}$ and $\sim 70\,\mathrm{km\ s^{-1}}$ for the primary and the secondary, respectively. One may question the apparently high values of F_1, F_2 given in Table 3. However note that they are defined relative to the average orbital angular rate, $\omega_{kepl} = 2\pi/P$. Comparison of the component's angular rotation rates and the orbital angular rate *at periastron* provides significantly smaller values, $\sim$0.5 (Gies et al. 1996). Indeed, combining the newly derived values of R_1 and R_2 for $i = 60^\circ$ with the observed values of $v_e\ sin\ i$ and assuming collinearity of the rotational and orbital axes, we obtain $F_1 = F_2 = 0.28$ at periastron.

6 CONCLUSIONS

Combining new, high-quality spectroscopic data with abundant photometric measurements spanning over two years, we derive a complete set of orbital parameters for the massive, highly eccentric O9III+B1III binary ι Orionis (Tables 2,3). The newly derived mass ratio, $q = m_1/m_2 = 1.75$, is somewhat lower than the value found by SPLH87, $q = 2.05$. We confirm the high rate of apsidal motion, with our new estimation $\dot{\omega} = (0.00049 \pm 0.00003)^\circ/\mathrm{day}$.

Separating the heavily blended spectra of the components, we were able to see signs of tidal interaction taking place during the very short interval of periastron passage, $\phi = 0.0 \pm 0.1$. To our surprise, we find no clear evidence of the bow shock crashing onto the secondary's surface even at periastron, i.e. presumably at the moment of maximum imbalance between the wind momenta.

The rapid, phase-locked photometric changes around periastron passage can be interpreted as arising from tidal deformations of the components (assuming that the shapes of the stars coincide with instantaneous equipotential Roche surfaces) and mutual illumination, without the necessity of invoking geometric eclipses. This leads to the relatively small values of the stellar radii (Table 3) and provides an estimate for the orbital inclination, $50^\circ \lesssim i \lesssim 70^\circ$.

7 ACKNOWLEDGEMENTS

SM is thankful to I. Hubeny for providing the most recent version of the TLUSTY code and on-line consultations. AFJM and SM wish to thank NSERC of Canada and FCAR of Québec for continuing financial support. GR and JMV acknowledge financial support by the Communauté Française (Belgium) and through contracts SSTC-PAI P4/05 and PRODEX XMM-OM. EA and IA acknowledge financial support from the Russian Foundation for Basic Research through grant No 99-02-17589. Ritter Observatory acknowledges grants from the Fund for Astrophysical Research and from the Small Grants Program of the American Astronomical Society (NASA funds). DB and NIM acknowledge the use at CASLEO of the CCD and data acquisition system supported by the US NSF grant AST-90-15827 to R.M. Rich. TE is grateful for full financial aid from the Evangelisches Studienwerk/Germany which is supported by the German Government, as well as for an extended bursary from the astronomy group at the Université de Montréal. The authors are grateful to the XMEGA community for the initial support while discussing and writing the ASCA proposal, and to M. Seeds (Brossman Center for Astronomy, USA) for the professional help in shaping and running the APT program.

REFERENCES

Antokhina E.A., 1996, Astronomy Reports, 40, 483
Antokhina E.A., Cherepashchuk A.M., 1994, Astronomy Reports, 38, 367
Bagnuolo W.G., Jr., Gies D.R., Hahula M.E., Wiemker R., Wiggs M.S., 1994, ApJ, 423, 446
Balog N.I., Goncharskii A.V., Cherepashchuk A.M., 1981, Sov. Astron. Letters, 7, 336
Conti P.S., 1974, ApJ, 187, 539
Corcoran M.F., 1996, Rev. Mex. AA, Ser. Conf., 5, 54
Corcoran M.F., Petre R., Swank J.H., Drake S.A., Koyama K., Tsuboi Y., Viotti R., Damineli A., Davidson K., Ishibashi K., White S., Currie D., 1998, ApJ, 494, 381
Gayley K.G., Owocki S.P., Cranmer S.R., 1997, ApJ, 475, 786
Gies D.R., Bagnuolo W.G., Jr., Penny L.R., 1997a, ApJ, 479, 408
Gies D.R., Barry D.J., Bagnuolo W.G., Jr., Sowers J., Thaller M.L., 1996, ApJ, 469, 884

Table 3. Parameters of the system calculated for different inclinations.

i deg	μ_1	μ_2	M_1 $M_\odot$	M_2 $M_\odot$	a $R_\odot$	R_1 $R_\odot$	R_2 $R_\odot$	F_1	F_2	L_1 erg s^{-1}	L_2 erg s^{-1}	$\Delta(o-c)$
30	0.65	0.30	120.	68.	229.	14.3	3.8	8.8	20 9	7.9×10^{38}	1.7×10^{37}	3.86
40	0.75	0.30	56.5	32.1	178.	13.3	3.0	7.4	20.9	6.8×10^{38}	1.0×10^{37}	2.42
45	0.75	0.30	42.4	24.0	162.	12.7	2.7	7.4	20.9	5.7×10^{38}	8.5×10^{37}	2.00
50	0.70	0.45	33.4	18.9	149.	10.3	4.7	8.0	11.2	4.1×10^{38}	2.5×10^{37}	1.81
55	0.70	0.50	27.3	15.5	140.	9.6	5.0	8.0	9.8	3.6×10^{38}	2.9×10^{37}	1.74
60	0.65	0.55	23.1	13.1	132.	8.3	5.4	8.8	8.7	2.6×10^{38}	3.3×10^{37}	1.73
65	0.55	0.65	20.2	11.4	126.	6.3	6.2	11.0	7.1	1.5×10^{38}	4.5×10^{37}	1.73
70	0.60	0.55	18.1	10.3	122.	6.9	5.0	9.8	8.7	1.8×10^{38}	2.8×10^{37}	1.77
75	0.60	0.35	16.6	9.4	118.	6.9	2.6	9.8	16.1	1.7×10^{38}	7.7×10^{36}	2.19
80	0.50	0.30	15.7	8.9	116.	5.1	1.2	12.7	2.9	9.9×10^{37}	4.4×10^{36}	3.11

Gies D.R., Mason B.D., Bagnuolo W.G., Hahula M.E., Hartkopf W.I., McAlister H.A., Thaller M.L., McKibben W.P., Penny L.R., 1997b, ApJ, 475, 49

Gies D.R., Wiggs M.S., Bagnuolo W.G., Jr., 1993, ApJ, 403, 752

Gordon K.D., Mulliss C.L., 1997, PASP, 109, 221

Hilditch R.W., Reynolds A.P., Bell S.A., Pollacco D.L., Edwin R.P., 1991, The Observatory, 111, 14

Howarth I.D., Siebert K.W., Hussain G.A.J., Prinja R.K., 1997, MNRAS, 284, 265

Hubeny I., Lanz T., 1992, A&A, 262, 501

Hubeny I., Lanz T., 1995, ApJ, 439, 875

Humphreys R.M., 1978, ApJS, 38, 309

Hutchings J.B., 1968, MNRAS, 141, 219

Miczaika G.R. 1951, Zeitschr. Astrophys., 29, 305

Moreno E., Koenigsberger G., 1999, RMA&A, in press

Pearce J.A., 1953, AJ, 58, 223

Pittard J.M., 1998, MNRAS, 300, 479

Pittard J.M., Stevens I.R., Corcoran M.F., Ishibashi K., 1998, MNRAS, 299, 5

Pittard J.M., Stevens I.R., Corcoran M.F., Marchenko S.V., Rauw G., Torii K., 1999, MNRAS, submitted

Plaskett J.S., Harper W.E., 1909, ApJ, 30, 373

Pollock A.M.T., Corcoran M.F., Stevens I.R., Williams P.M., van der Hucht K.A., 1995, in van der Hucht K.A., Williams P.M., eds., Proc. IAU Symp. 163, Wolf-Rayet stars: binaries, colliding winds, evolution, kluwer, Dordrecht, 510

Rauw, G., Vreux, J.-M., Bohannan, B., 1999, ApJ, 517, 416

Schmidt-Kaler Th., 1982, in Schaiffers K., Voigt H.H., eds., Numerical data and functional relationships in science and technology, Group 6, Vol. 2b, Springer, Berlin, 1

Shore S.N., Brown D.N., 1988, ApJ, 334, 1021

Stevens I.R., 1988, MNRAS, 235, 523

Stevens I.R., Blondin, J.M, Pollock A.M.T., 1992, ApJ, 386, 265

Stevens I.R., Corcoran M.F., Willis A.J., Skinner S.L., Pollock A.M.T., Nagase F., Koyama K., 1996, MNRAS, 283, 589

Stevens I.R., Howarth I.D., 1999, MNRAS, 302, 549

Stickland D.J., Pike C.D., Lloyd C., Howarth I. D., 1987, A&A, 184, 185

Van Hamme W., 1993, AJ, 106, 2096

Walborn N.R., 1980, ApJS, 44, 535

Walder, R.,& Folini, D. 1998, A&A, 330, L21

Wiggs M.S., Gies D.R., 1992, ApJ, 396, 238

Wiggs M.S., Gies D.R., 1993, ApJ, 407, 252

Willis A.J., Schild H., Stevens I.R., 1995, A&A, 298, 549

Wilson R.E., 1979, ApJ, 234, 1054

Wolfe R.H.Jr., Horak H.G., Storer N.W. 1967, in Hack M., ed., Modern Astrophysics, Gordon & Breach, New York, 251

Young A.I., Genet R.M., Boyd L.J., et al., 1991, PASP, 103, 221